

- Supporting Information -

Role of Architecture on Thermorheological Properties of Poly(alkyl methacrylate)-Based Polymers

Bas G. P. van Ravensteijn^{†,‡,†}, Raghida Bou Zerdan^{†,‡}, Craig J. Hawker^{§,‡,#}, Matthew E. Helgeson^{‡,*}

[‡]Department of Chemical Engineering, [†]Materials Research Laboratory, [§]Department of Chemistry and Biochemistry, [#]Materials Department, University of California, Santa Barbara, California 93106, United States.

* E-mail: helgeson@engineering.ucsb.edu

Table of contents

S1	Overview of employed p(SMA- <i>co</i> -MMA)-based rheological modifiers.....	S-2
S2	Size exclusion chromatography – multi angle light scattering analysis	S-3
S3	Viscosity data used for calculation of the VI (rheometer).....	S-5
S4	Estimation of overlap concentration c^* for the p(SMA- <i>co</i> -MMA) additives.....	S-6
S5	Kraemer and Huggins extrapolations of viscosity data to determine $[\eta]$	S-7
S6	SANS profiles and Guinier analysis for <i>linear</i> p(SMA- <i>co</i> -MMA) and <i>IC-Star</i> ₉	S-11
S7	Fitting of small angle neutron scattering profiles.....	S-12
S8	Dynamic light scattering correlation functions and size distributions.....	S-16
S9	Scattered intensity in dynamical light scattering: HD vs. YB4 as solvent.....	S-18
S10	Concentration dependence of DLS correlation functions and size distributions.....	S-18

S1 Overview of employed p(SMA-co-MMA)-based viscosity modifiers

Table S1. Relevant physical characteristics of p(SMA-co-MMA)-based viscosity improvers.

Entry	Additive	SMA: MMA ^a	X [%]	$M_{w,th}$ [kg·mol ⁻¹] ^b	Absolute M_w [kg·mol ⁻¹] ^c	M_n [kg·mol ⁻¹] ^c	\mathcal{D} [-] ^d	R_g [nm] ^c
1	<i>Linear</i>	370:370	99	165	170	110	1.5	11.6 ± 0.7
2	<i>Branched</i>	—	—	—	130	70	1.9	10.3 ± 1.6
3	<i>OC-star₈</i>	50:50	50	352	180	150	1.2	8.2 ± 0.1
4	<i>IC-star₉</i>	60:65	64	393	300	230	1.3	11.0 ± 0.4

^a Monomer incorporation ratio determined by ¹H NMR analysis of diagnostic signals of stearyl methacrylate (SMA) at 3.9 ppm and methyl methacrylate (MMA) at 3.6 ppm with respect to the corresponding isolated initiator peaks. For star polymers, the ratios per arm are listed. Ratios are reported with a maximum of two significant figures to account for the uncertainty accompanied to integrating NMR signals. ^b Determined based on total monomer consumption. ^c Determined using size exclusion chromatography-multi angle laser scattering (SEC-MALS) in chloroform; see Supporting Information S2. ^d Calculated using $\mathcal{D} = M_w/M_n$. See Reference S1 for details.

S2 Size exclusion chromatography – multi angle light scattering analysis

S2.1. Experimental details. The chromatography instrument comprised a Waters Alliance HPLC 2695 separation module in combination with two 300×7.8 mm, $5 \mu\text{m}$ 2 Agilent PolyPore GPC columns (flow rate = $1 \text{ mL}\cdot\text{min}^{-1}$) coupled to a Wyatt DAWN HELEOS-II light scattering detector ($\lambda_0 = 663.1$ nm) and a Wyatt Optilab rEX differential refractive index (dRI) detector. Chloroform with 0.25% triethylamine (TEA) was used as the mobile phase and measurements were performed at $30 \text{ }^\circ\text{C}$. One hundred microliters of a polymer solution with known concentration ($3\text{--}5 \text{ mg}\cdot\text{mL}^{-1}$) was injected for analysis. The resulting light-scattering data were analyzed following a partial Zimm formalism developed for static light-scattering (SLS) of dilute solutions of noninteracting polymers.

S2.2. Variance in R_g per polymer. To confirm the larger spread in coil dimensions and verify that our polymers have a monomodal size distribution, we performed SEC-multi-angle light scattering (MALS) experiments. With this technique, molecular weight distributions and coil dimensions ((as reflected by the radius of gyration, R_g) can be determined simultaneously at any given point in this distribution. The resulting light scattering and differential refractive index (dRI) chromatograms are depicted below. All of the employed polymers show monomodal size distributions.

Please note that for the linear and star polymers, the light scattering trace revealed a small shoulder at lower retention times (Figure S1a and c, respectively). This shoulder is caused by a low concentration of coupled polymers formed during synthesis.^{S1} Light scattering is significantly more sensitive towards these larger objects than dRI detection. Given that the couple products are hardly observed in the dRI signal, implies a low concentration of these higher molecular weight side products. The positions where R_g was evaluated are highlighted Figure S1 in gray. Table S2 lists the values for R_g for both regions of interest. Considering the low light scattering intensity at the extremes of the chromatograms, the obtained R_g 's should only be treated as an indicative value. Despite a small mismatch between the values for R_g and R_h (reported in main text), the spread in coil sizes are comparable. Deviations in coil sizes are caused by the different definitions of R_g and R_h , the fact that DLS will be more sensitive to

conformational fluctuations at a given molecular weight, and the fact that the DLS and GPC-MALS experiments were performed in different solvents (*n*-hexadecane / YB4 with respect to chloroform).

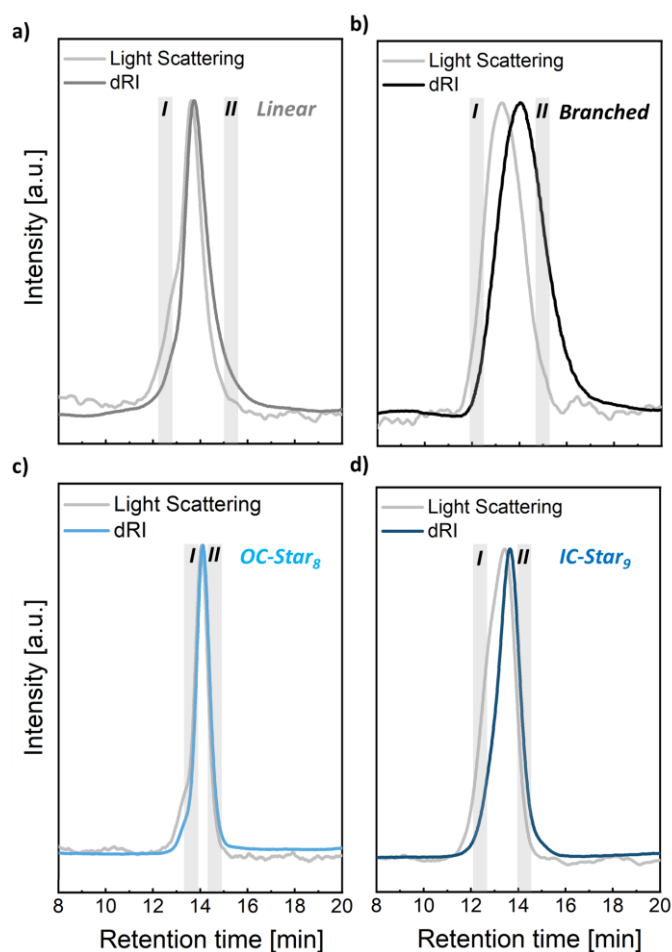


Figure S1. Size exclusion chromatography – multi angle light scattering (SEC-MALS) traces of p(SMA-co-MMA) based polymers. a) *linear*, b) *branched*, c) organic stars carrying 8 arms (*OC-Star₈*), d) hybrid stars carrying an average of 9 arms (*IC-Star₉*). Both the differential refractive index (dRI) and light scattered signal are shown. The radii of gyration (R_g) are determined at both ends of the chromatograms, as indicated with the gray shaded regions *I* and *II*.

Table S2. Limiting values for the radii of gyration as measured with size exclusion chromatography – multi angle light scattering (SEC-MALS) for the library of p(SMA-co-MMA)-derived polymers.

Entry	Polymer	Lower R_g limit (region <i>I</i>) [nm]	Upper R_g limit (region <i>II</i>) [nm]
1	<i>Linear</i>	5.7	28.5
2	<i>Branched</i>	4.7	28.0
3	<i>OC-Star₈</i>	4.1	12.6
4	<i>IC-Star₉</i>	7.4	26.4

S3 Viscosity data used for calculation of the VI (rheometer)

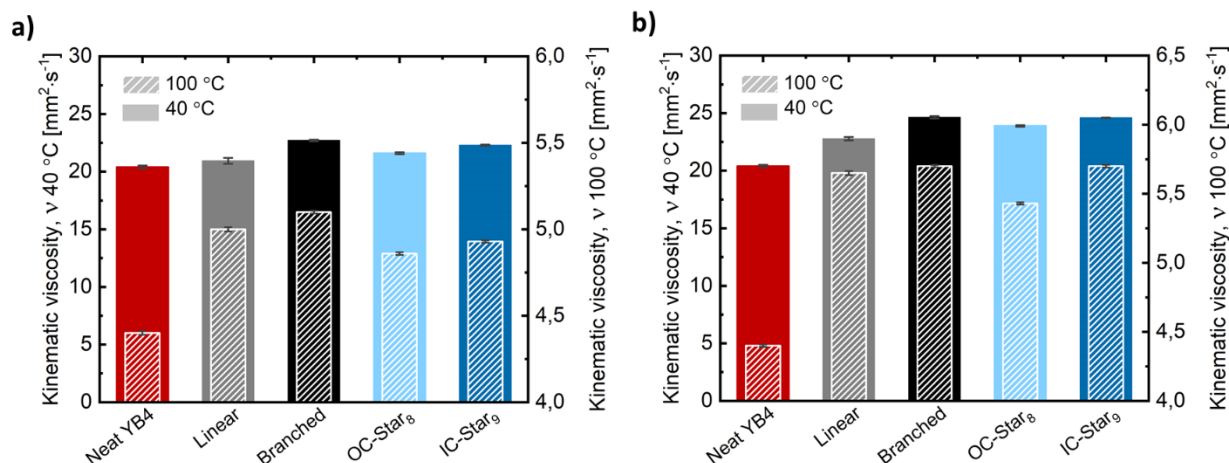


Figure S2. Kinematic viscosities (ν) at 40 °C (filled bars, left y -axis) and 100 °C (stipped bars, right y -axis) of pure Yubase 4 (YB4, red) and its solution containing a) 1 wt% or b) 2 wt% poly(stearyl methacrylate-*co*-methyl methacrylate) (p(SMA-*co*-MMA)) derived additives. The error bars represent the error associated with the extrapolation of the shear-dependent measurements to obtain the zero-shear viscosity. Gray: *linear* p(SMA-*co*-MMA), black: *branched* p(SMA-*co*-MMA), light blue: organic stars carrying 8 arms (*OC-Star*₈), dark blue: hybrid stars carrying an average of 9 arms (*IC-Star*₉).

Table S3. Kinematic viscosities of 1 and 2 wt% p(SMA-*co*-MMA)-based polymer solutions at 40 and 100 °C.

Entry	Polymer	Kinematic viscosity [mm ² · s ⁻¹] 1 wt% solutions		Kinematic viscosity [mm ² · s ⁻¹] 2 wt% solutions	
		$T = 40\text{ °C}$	$T = 100\text{ °C}$	$T = 40\text{ °C}$	$T = 100\text{ °C}$
1	-	20.4 ± 0.1	4.4 ± 0.01	20.4 ± 0.1	4.4 ± 0.01
2	<i>Linear</i>	20.9 ± 0.3	5.0 ± 0.01	22.8 ± 0.2	5.7 ± 0.02
3	<i>Branched</i>	22.7 ± 0.1	5.1 ± 0.01	24.6 ± 0.1	5.7 ± 0.01
4	<i>OC-star</i> ₈	21.6 ± 0.1	4.9 ± 0.01	23.9 ± 0.1	5.4 ± 0.01
5	<i>IC-star</i> ₉	22.3 ± 0.1	4.9 ± 0.01	24.6 ± 0.2	5.7 ± 0.01

S4 Estimation of overlap concentration c^* for the p(SMA-*co*-MMA) additives

The overlap concentrations (c^*) of the employed p(SMA-*co*-MMA) polymers were estimated using the following equation:^{S2}

$$c^* = \frac{M_w}{\frac{4}{3}\pi R_g^3 N_A} \quad (\text{S1})$$

where M_w represents the molecular weight of the polymer, R_g the radius of gyration, and N_A Avagadro's number. For the calculation, absolute molecular weights were used (Table S1) as previously measured using size exclusion chromatography-multi angle light scattering (SEC-MALS).^{S1} R_g values from SANS measurements performed in *n*-hexadecane- d_{34} (*d*-HD) at 25 °C and 90 °C were taken. The results are summarized in Table S4.

Table S4. Estimation of the overlap concentration (c^*) for the p(SMA-*co*-MMA) based viscosity improvers.

Entry	Additive	R_g [nm] ^d		Absolute M_w [kg·mol ⁻¹]	c^* [mg/mL]	
		$T = 25$ °C	$T = 90$ °C		$T = 25$ °C	$T = 90$ °C
1	<i>Linear</i>	5.9	6.9	170	330	200
2	<i>Branched</i>	5.3	6.4	130	350	200
3	<i>OC-star₈</i>	7.3	8	180	180	140
4	<i>IC-star₉</i>	6.4	7	300	450	350

As these estimations are significantly higher compared to the maximal applied polymer concentration (25 mg/mL = 3 wt%), it was assumed that all experiments were performed in the dilute concentration regime.

S5 Kraemer and Huggins extrapolations of viscosity data to determine $[\eta]$

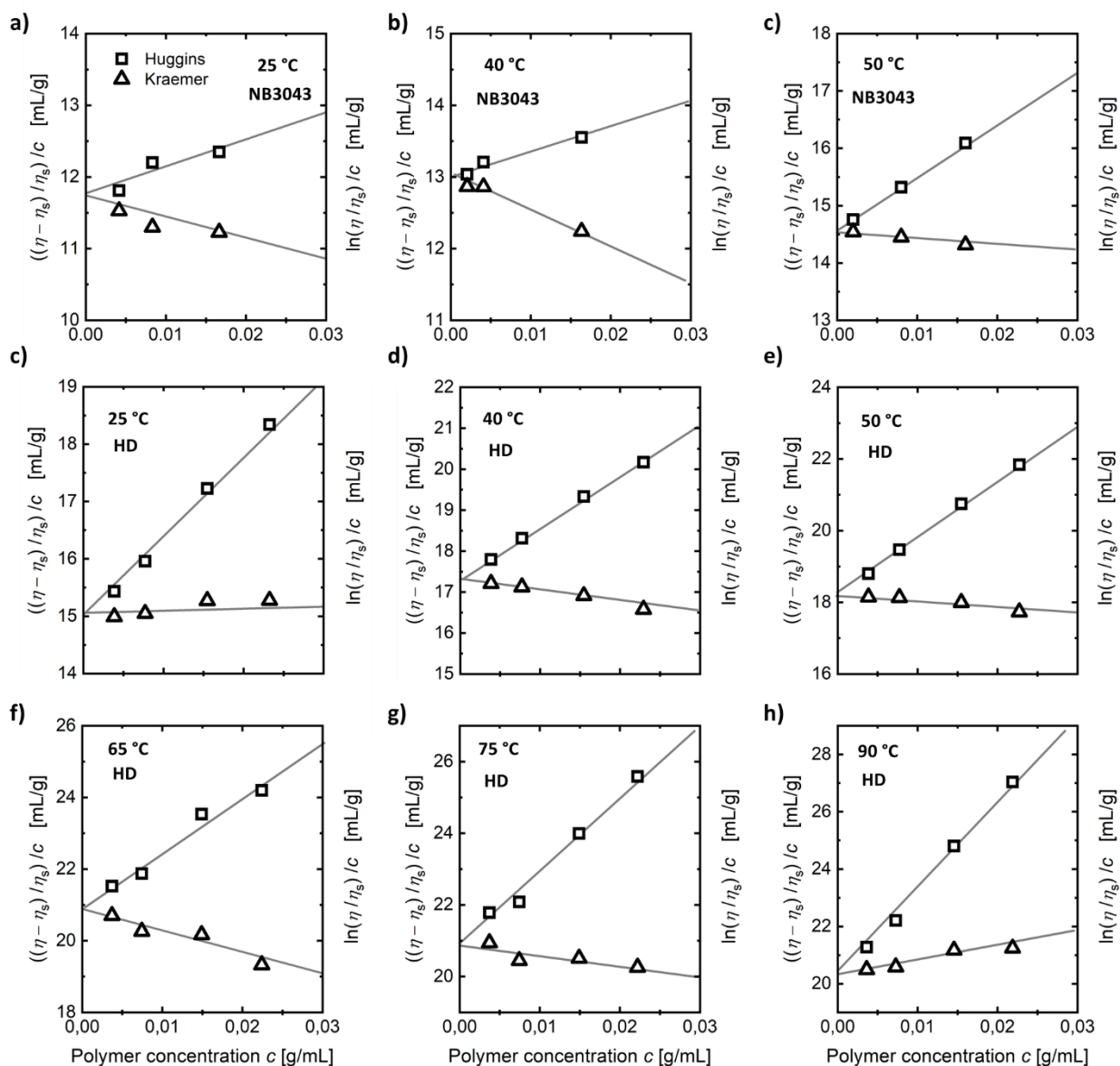


Figure S3. Huggins (squares) and Kraemer (triangles) extrapolations for the *branched* poly(stearyl methacrylate-*co*-methyl methacrylate) (p(SMA-*co*-MMA)) additives dissolved in Nexbase 3043 (NB3043) at a) 25, b) 50, and c) 75 °C. Huggins and Kraemer extrapolations of *branched* (p(SMA-*co*-MMA)) dissolved in *n*-hexadecane (HD) at c) 25, d) 40, e) 50, f) 65, g) 75, and h) 90 °C.

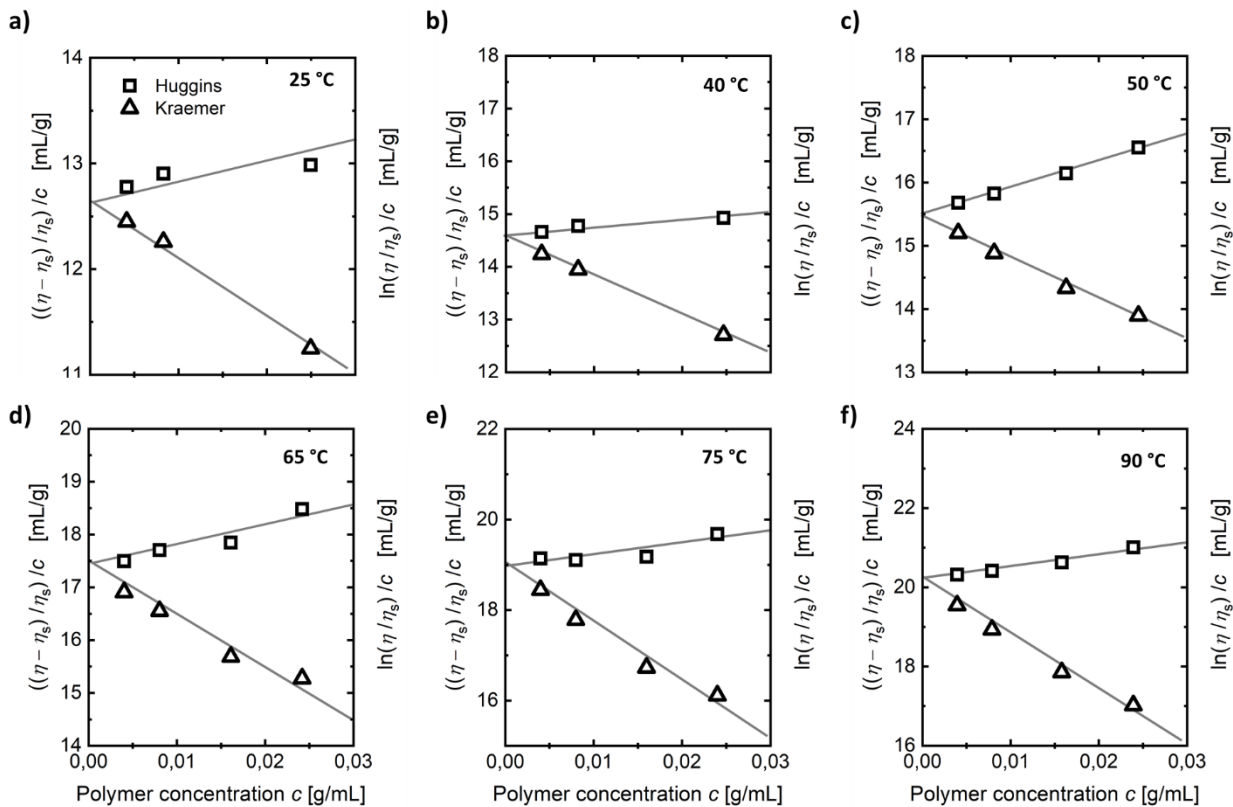


Figure S4. Huggins (squares) and Kraemer (triangles) extrapolations for the *branched* poly(stearyl methacrylate-*co*-methyl methacrylate) (p(SMA-*co*-MMA)) additives dissolved in Yubase 4 (YB4) at a) 25, b) 40, c) 50, d) 65, e) 75, and f) 90 °C.

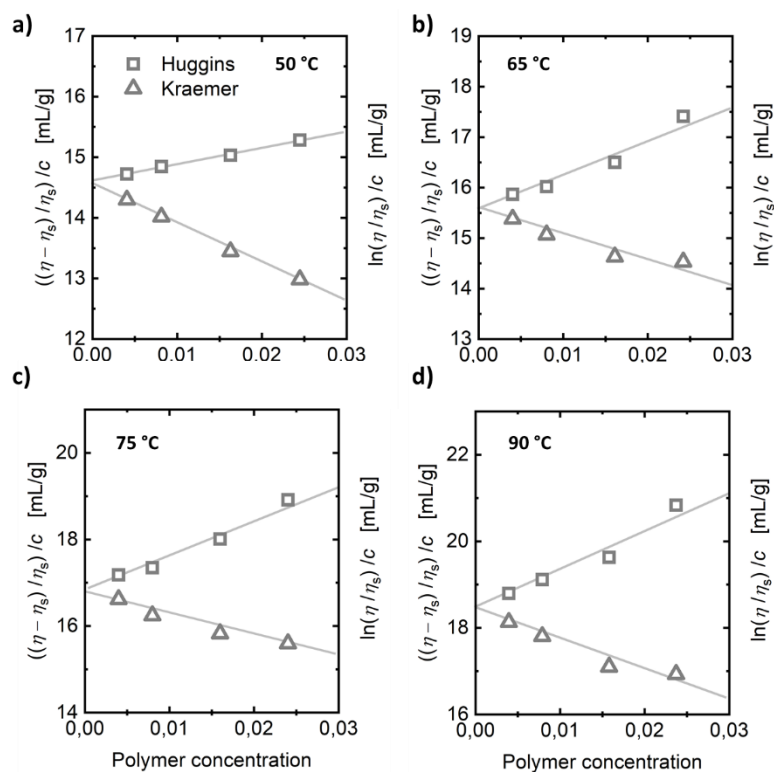


Figure S5. Huggins (squares) and Kraemer (triangles) extrapolations for *linear* poly(stearyl methacrylate-*co*-methyl methacrylate) (p(SMA-*co*-MMA)) additives in Yubase 4 (YB4) at a) 50, b) 65, c) 75 and d) 90 °C.

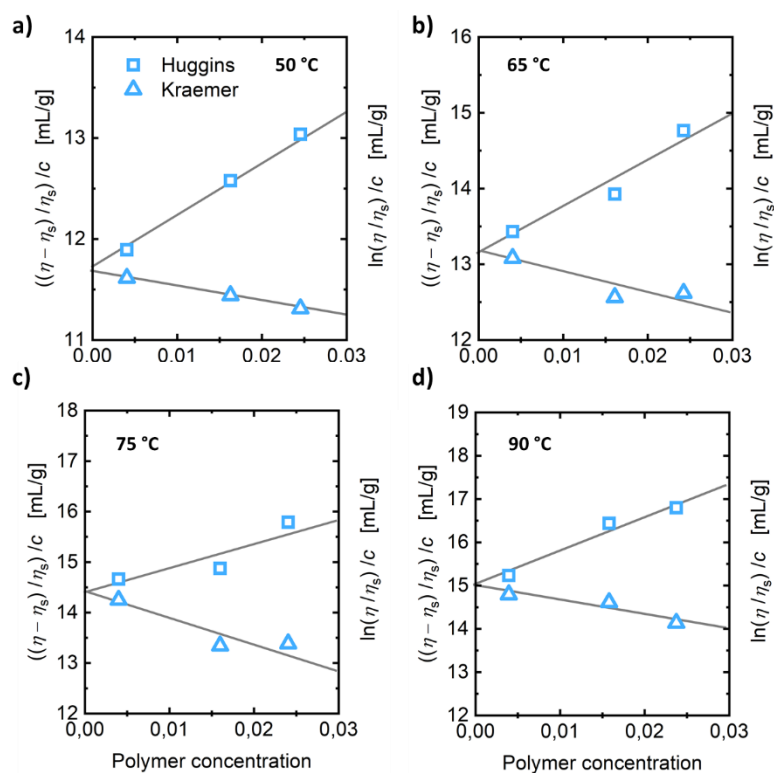


Figure S6. Huggins (squares) and Kraemer (triangles) extrapolations for the fully organic, star-shaped poly(stearyl methacrylate-*co*-methyl methacrylate) (p(SMA-*co*-MMA))-based additives (*OC-Star*₈) dissolved in Yubase 4 (YB4) at a) 50, b) 65, c) 75 and d) 90 °C.

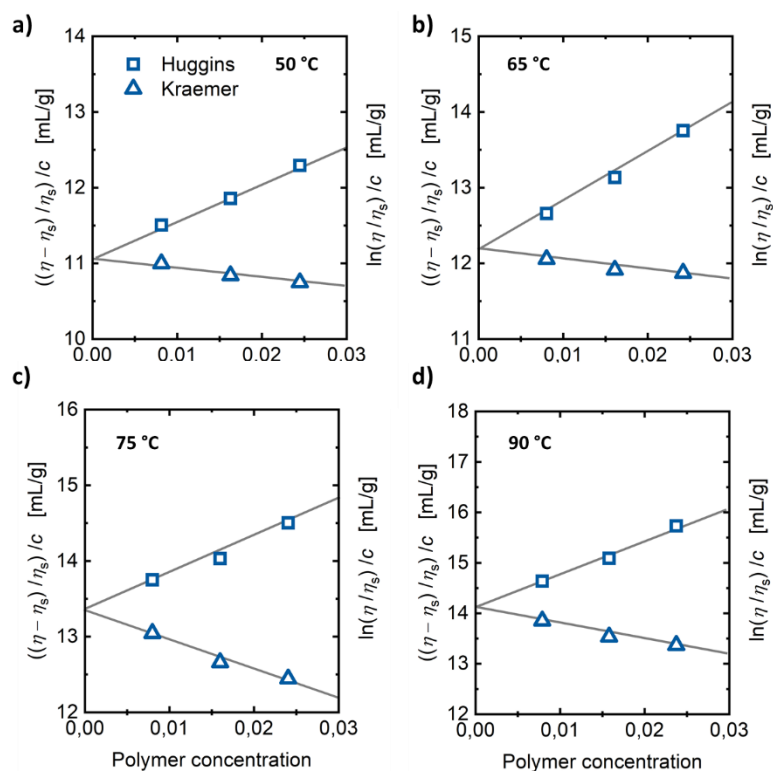


Figure S7. Huggins (squares) and Kraemer (triangles) extrapolations for the hybrid organic-inorganic star-shaped poly(stearyl methacrylate-*co*-methyl methacrylate) (p(SMA-*co*-MMA))-based additives (*IC-Star*₉) in Yubase 4 (YB4) at a) 50, b) 65, c) 75 and d) 90 °C.

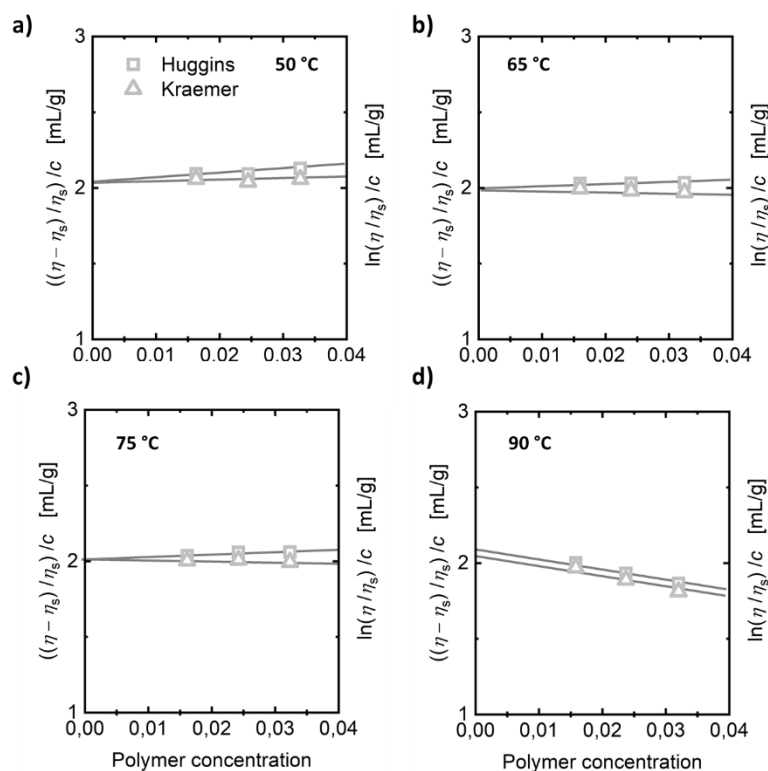


Figure S8. Huggins (squares) and Kraemer (triangles) extrapolations for additives comprised of cross-linked silicate cores dissolved in Yubase 4 (YB4) at a) 50, b) 65, c) 75 and d) 90 °C.

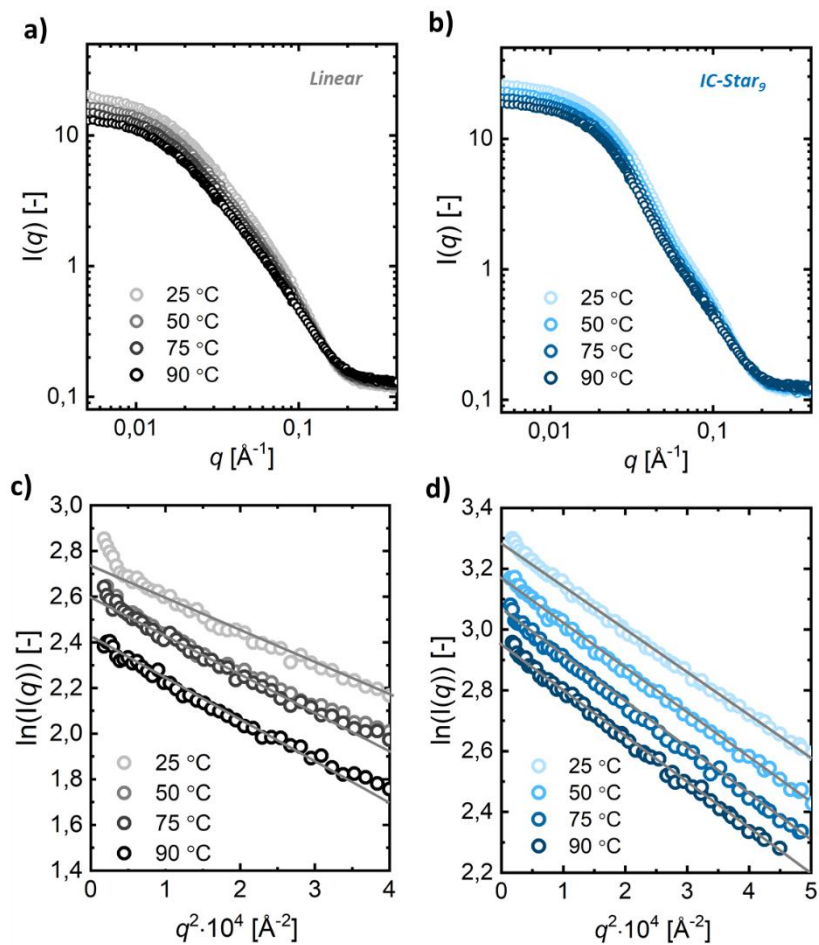


Figure S9. Small angle neutron scattering (SANS) profiles as a function of temperature for a) linear and b) the hybrid star-shaped (*IC-Star*₉) poly(stearyl methacrylate-*co*-methyl methacrylate) (p(SMA-*co*-MMA)) additives. Guinier analysis of SANS profiles depicted in c) panel a and d) in panel b. Measurements were performed in *n*-hexadecane-*d*₃₄ (*d*-HD) as solvent.

S7 Fitting of small angle neutron scattering profiles

S7.1. Fitting SANS profiles for branched p(SMA-co-MMA). As explained in the main text, the radii of gyration (R_g) for the randomly branched polymers could not be determined following the Guinier approximation due to an upturn of the scattering intensity in the low q -regime. Alternatively, values for R_g are determined by fitting the scattering profiles with a model suitable for polymers with excluded volume interactions.^{S3,S4} The structure factor ($P(q)$) in this case is given by

$$P(q) = \frac{1}{\nu U^{1/2\nu}} \gamma\left(\frac{1}{2\nu}, U\right) - \frac{1}{\nu U^{1/\nu}} \gamma\left(\frac{1}{\nu}, U\right) \quad (\text{S2a})$$

$$\gamma(x, U) = \int_0^U dt \exp(-t) t^{x-1} \quad (\text{S2b})$$

$$U = \frac{q^2 R_g^2 (2\nu + 1)(2\nu + 2)}{6} \quad (\text{S2c})$$

where q is the scattering vector, ν represents the excluded volume parameter, and R_g the radius of gyration. The low q -regime ($0.004 < q < 0.01$) was excluded during the fitting procedure. Figure S10 depicts an overlay of the scattering profiles obtained at 25, 50, 75, and 90 °C (gray data points) and excluded volume fit (red curves). The parameters that ensured the best fit to the experimental data are listed in Table S5.

Table S5. Fitting parameters of excluded volume model for branched p(SMA-co-MMA) additives.

Entry	Temperature [°C]	Scale [-]	Background [cm ⁻¹]	R_g [nm]	Excluded volume parameter ν [-]
1	25	9.2 ± 0.02	0.066 ± 8 · 10 ⁻⁴	5.2 ± 0.06	0.40 ± 0.006
2	50	7.9 ± 0.03	0.055 ± 7 · 10 ⁻⁴	5.5 ± 0.2	0.45 ± 0.007
3	75	7.6 ± 0.03	0.066 ± 2 · 10 ⁻⁴	5.9 ± 0.2	0.46 ± 0.005
4	90	9.5 ± 0.03	0.086 ± 7 · 10 ⁻⁴	6.4 ± 0.2	0.48 ± 0.006

Evidently, R_g increases with temperature. Additionally, the ν increases upon heating. Excluded volume exponents equal to $1/3$ are associated with collapsed polymer chains in a moderate to poor solvent, while $\nu = 3/5$ and $1/2$ and correspond to a fully swollen and Gaussian chain conformation, respectively. Therefore, the measured increase in ν suggests a temperature-induced enhancement of the solvent quality and increasingly more swollen polymer coil structure, given nearly Gaussian coils at 90 °C.

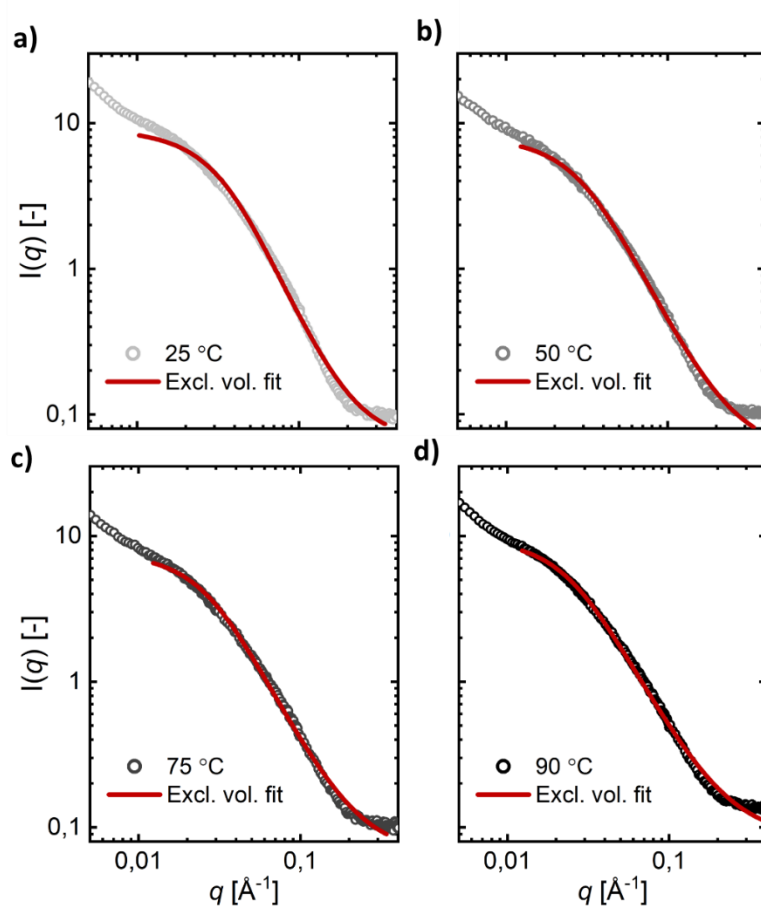


Figure S10. Small angle neutron scattering (SANS) profiles of the branched poly(stearyl methacrylate-*co*-methyl methacrylate) (p(SMA-*co*-MMA)) additive (gray points) and corresponding fits (red curves) of the experimental data with a model describing the scattering of polymers with excluded volume interactions at a) 25, b) 50 , c) 75, and d) 90 °C Measurements were performed in *n*-hexadecane- d_{34} (*d*-HD) as solvent.

S7.2. Fitting SANS profiles for *IC-Star*₉. The SANS profiles for the star-shaped additives showed a distinct structural feature located at approximately $q = 0.1 \text{ \AA}^{-1}$. To confirm that this feature is associated with the star architecture, the profiles were fitted to a model developed by Dozier et al. and modified by Molina et al describing the scattering from monodisperse star polymers:^{S5,S6}

$$nV^2\Delta\rho^2P_{\text{star}}(q) = I_{G-P}(q) + \frac{4\pi\alpha \sin[\mu \tan^{-1}(q\xi)]}{q\xi [1 + q^2\xi^2]^{\mu/2}}\Gamma(\mu) \quad (\text{S3a})$$

The first term on the right-hand side of Eq. S3a is a low- q Guinier–Porod contribution to the scattering intensity for aggregates with radius of gyration R_g , given by

$$I_{G-P}(q) = I(0)^S \exp\left(\frac{-q^2R_g^2}{3}\right) \quad \text{for } q \leq \sqrt{6/R_g} \quad (\text{S3b})$$

$$I_{G-P}(q) = I(0)^S \frac{36e^{-2}}{q^4R_g^4} \quad \text{for } q > \sqrt{6/R_g} \quad (\text{S3c})$$

where $I(0)^S$ is the scale factor for the star scattering. The second term accounts for the blob–blob correlation of star arms according to the Daoud–Cotton model with blob size ξ , scaling parameter α , $\mu = \nu^{-1} - 1$,^{S6} and $\Gamma(\mu)$ the gamma function with argument μ . The star scattering is then modeled using the deconvolution approximation:

$$I(q) = nV^2\Delta\rho^2P_{\text{star}}(q)S(q) \quad (\text{S4})$$

where n and V are the number density and volume of individual stars, respectively. $\Delta\rho$ is the scattering length density contrast, and $P_{\text{star}}(q)$ and $S(q)$ are the form and structure factors, respectively. As the polymer solution considered here are dilute, $S(q) = 1$.

Figure S11 shows the excellent agreement between the experimental data (blue data points) and the Dozier model for the scattering profile obtained for *IC-Star*₉ at 25 °C. The parameters used to generate this fit are listed in Table S6. Similar levels of fitting accuracy could be obtained for the profiles obtained at the other temperatures and for the organic p(SMA-*co*-MMA)-based star polymer. The radii of gyration are in close agreement to the values obtained with a Guinier analysis.

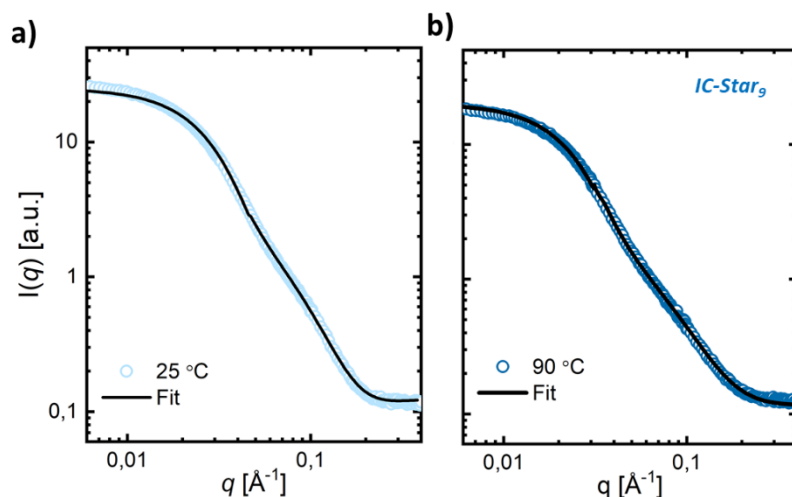


Figure S11. Small angle neutron scattering (SANS) profiles of the hybrid star-shaped (*IC-Star₉*) poly(stearyl methacrylate-*co*-methyl methacrylate) (p(SMA-*co*-MMA)) additive (blue points) and corresponding fits (black curves) of the experimental data with the Dozier model for star-shaped polymers at a) 25 and b) 90 °C. Measurements were performed in *n*-hexadecane-*d*₃₄ (*d*-HD) as solvent.

Table S6. Fitting parameters of Dozier model for *IC-Star₉*.

Entry	Temperature [°C]	Guinier – Porod regime					High <i>q</i> -regime				
		<i>R_g</i> [nm]	ξ [nm]	μ [-]	ν [-]	α [-]	<i>R_g</i> [nm]	ξ [nm]	μ [-]	ν [-]	α [-]
1	25	6.3	7.4	3.1	0.24	0.012	6.1	7.5	3.1	0.24	0.012
2	90	7.2	9.5	2.3	0.30	0.022	7.2	9.5	2.3	0.30	0.022

S8 Dynamic light scattering correlation functions and size distributions

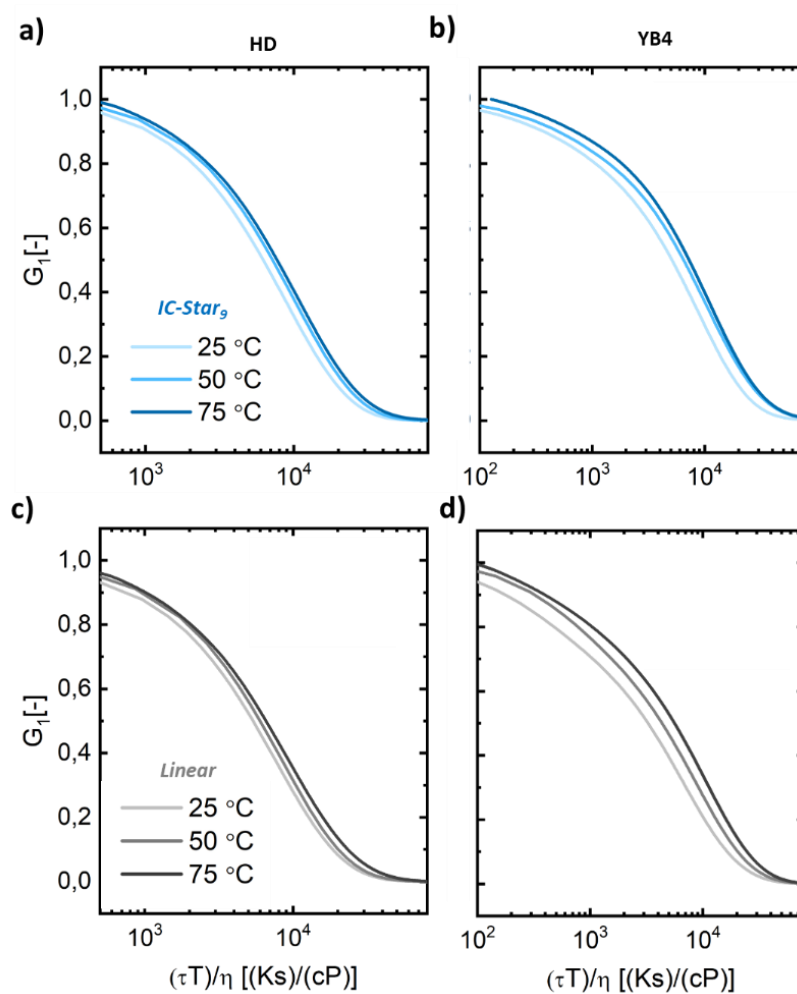


Figure S12. Normalized correlation functions as function of temperature obtained using dynamic light scattering (DLS) for poly(stearyl methacrylate-*co*-methyl methacrylate) (p(SMA-*co*-MMA)) hybrid star polymers (*IC-Star*₉) in a) *n*-hexadecane (HD) and b) Yubase 4 (YB4). DLS correlations functions of *linear* p(SMA-*co*-MMA) in c) HD and d) YB4.

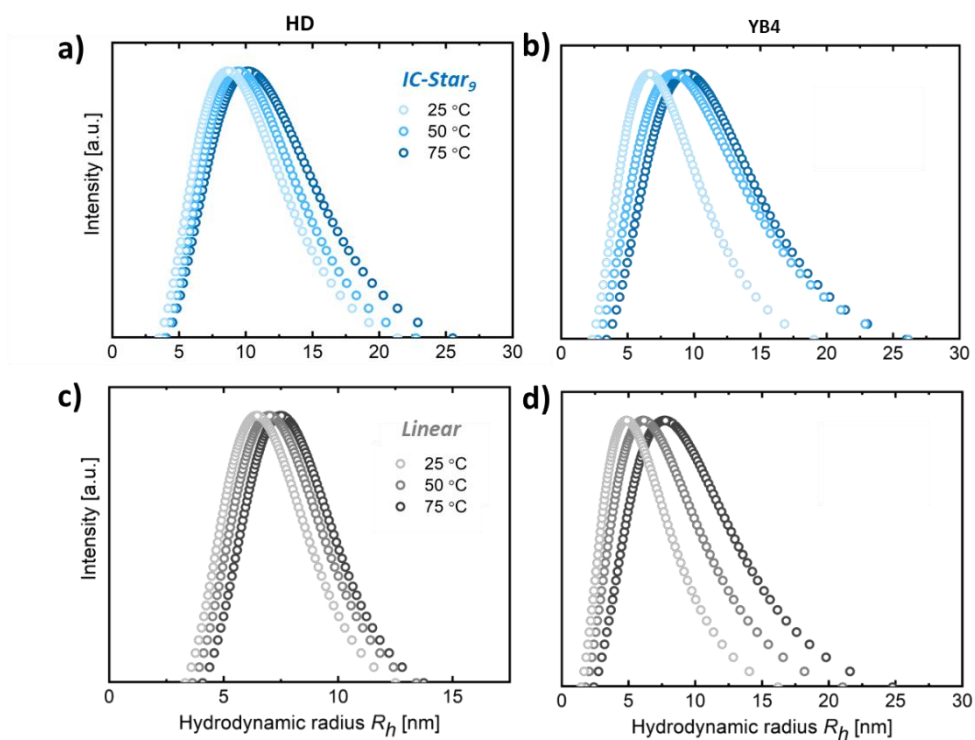


Figure S13. Intensity weighted size distributions measured with dynamic light scattering (DLS) for poly(stearyl methacrylate-*co*-methyl methacrylate) (p(SMA-*co*-MMA)) hybrid star polymers (*IC-Star*₉) in a) *n*-hexadecane (HD) and b) Yubase 4 (YB4). Analogous size distributions for the *linear* p(SMA-*co*-MMA) in c) HD and d) YB4. Distributions of the hydrodynamic radius (R_h) versus intensity were obtained from the correlation functions shown in Figure S12.

S9 Scattered intensity in dynamical light scattering: HD vs. YB4 as solvent

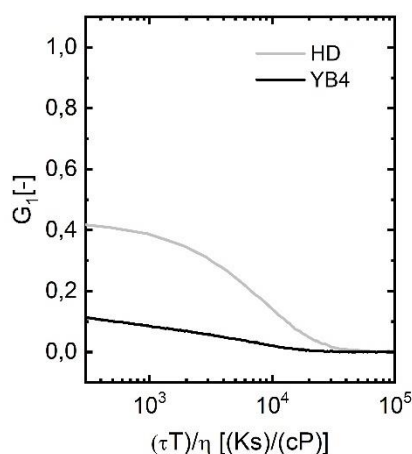


Figure S14. Non-intensity normalized correlation functions (G_1) obtained using dynamic light scattering (DLS) for the randomly branched poly(stearyl methacrylate-*co*-methyl methacrylate) (p(SMA-*co*-MMA)) additive in *n*-hexadecane (HD, light gray) and Yubase 4 (YB4, black). For both measurements the polymer concentration was equal to 10 mg/mL. Compared to the HD-based solutions, the scattering intensity decreases significantly when employing YB4 as solvent.

S10 Concentration dependence of DLS correlation functions and size distributions

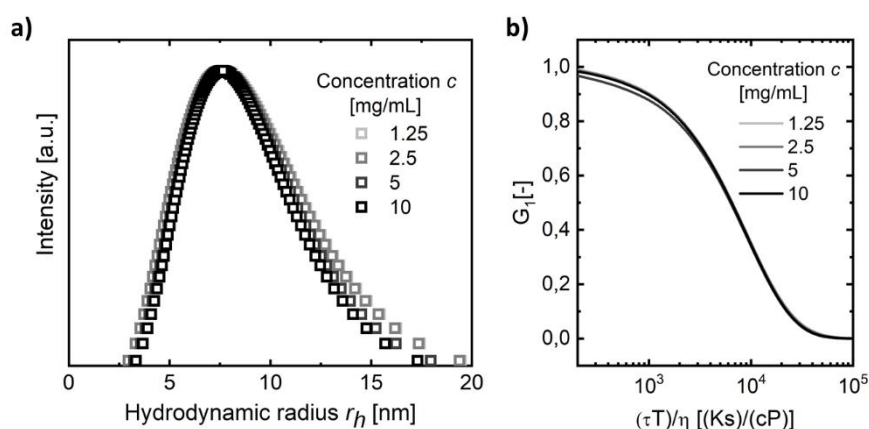


Figure S15. Intensity weighted size distributions measured with dynamic light scattering (DLS) for the randomly branched poly(stearyl methacrylate-*co*-methyl methacrylate) (p(SMA-*co*-MMA)) additive as function of the polymer concentration (c) in *n*-hexadecane (HD) at a constant temperature of 25 °C. b) Normalized correlation functions of the size distributions depicted in panel a.

References

- (S1) Van Ravensteijn, B. G. P.; Bou Zerdan, R.; Seo, D.; Cadirov, N.; Watanabe, T.; Gerbec, J. A.; Hawker, C. J.; Israelachvili, J. N.; Helgeson, M. E. Triple function lubricant additives based on organic-inorganic hybrid star polymers: Friction reduction, wear protection, and viscosity modification. *ACS Appl. Mater. Interfaces* **2019**, *11* (1), 1363–1375.
- (S2) Rubinstein, M.; Colby, R. H. In *Polymer Physics. 1st ed.*; Oxford University Press Inc., New York, NY, **2003**.
- (S3) Hammouda, B. SANS from homogeneous polymer mixtures – A unified overview, *Advances in Polym. Sci.* **1993**, *106*, 87–133.
- (S4) Hammouda, B.; Kim, M.-H. The empirical core-chain model. *J. Mol Liq.* **2017**, *247*, 434–440.
- (S5) Dozier, W. D.; Huang, J. S.; Fetters, L. J. Colloidal nature of star polymer dilute and semi-dilute solutions. *Macromolecules* **1991**, *24* (10), 2810–2814.
- (S6) Molina, P. M.; Lad, S.; Helgeson, M. E. Heterogeneity and its influence on the properties of difunctional poly(ethylene glycol) hydrogels: Structure and mechanics. *Macromolecules* **2015**, *48* (15), 5402–5411.